

Article

Gas Transport Model in Organic Shale Nanopores Considering Langmuir Slip Conditions and Diffusion: Pore Confinement, Real Gas, and Geomechanical Effects

Liehui Zhang ¹, Baochao Shan ^{1,*}, Yulong Zhao ^{1,*}, Jia Du ², Jun Chen ¹ and Xiaoping Tao ³

¹ State Key Laboratory of Oil and Gas Reservoir Geology and Exploitation, Southwest Petroleum University, Chengdu 610500, China; zhangliehui@vip.163.com (L.Z.); chenjunswpu@swpu.edu.cn (J.C.)

² Research Center of China United Coalbed Methane Corporation, Ltd., Beijing 100011, China; dujia83@hotmail.com

³ Xinjiang Oilfield Company Capital Construction Engineering, Karamay, Xinjiang 834000, China; taoxiaop@petrochina.com.cn

* Correspondence: rzshan@foxmail.com (B.S.); swpuzhao@swpu.edu.cn (Y.Z.);
Tel.: +86-177-6121-6601 (B.S.); +86-159-8232-4747 (Y.Z.)

Received: 3 December 2017; Accepted: 12 January 2018; Published: 17 January 2018

Abstract: Nanopores are extremely developed and randomly distributed in shale gas reservoirs. Due to the rarefied conditions in shale strata, multiple gas transport mechanisms coexist and need further understanding. The commonly used slip models are mostly based on Maxwell slip boundary condition, which assumes elastic collisions between gas molecules and solid surfaces. However, gas molecules do not rebound from solid surfaces elastically, but rather are adsorbed on them and then re-emitted after some time lag. A Langmuir slip permeability model was established by introducing Langmuir slip BC. Knudsen diffusion of bulk phase gas and surface diffusion of adsorbed gas were also coupled into our nanopore transport model. Considering the effects of real gas, stress dependence, thermodynamic phase changes due to pore confinement, surface roughness, gas molecular volume, and pore enlargement due to gas desorption during depressurization, a unified gas transport model in organic shale nanopores was established, which was then upscaled by coupling effective porosity and tortuosity to describe practical SGR properties. The bulk phase transport model, single capillary model, and upscaled porous media model were validated by data from experimental data, lattice Boltzmann method or model comparisons. Based on the new gas transport model, the equivalent permeability of different flow mechanisms as well as the flux proportion of each mechanism to total flow rate was investigated in different pore radius and pressure conditions. The study in this paper revealed special gas transport characteristics in shale nanopores and provided a robust foundation for accurate simulation of shale gas production.

Keywords: apparent permeability model; Knudsen diffusion; Langmuir slip condition; shale gas reservoir; surface diffusion

1. Introduction

In recent decades, shale gas has drawn great attention globally, especially with its successful development in North America [1–3]. As a typical unconventional energy resource, shale gas transport mechanisms in organic shale nanopores display a number of unique characteristics; for example, the slippage effect, Knudsen diffusion, surface diffusion, and adsorption/desorption behaviors [4,5]. These unique transport mechanisms enhance the flow capability of shale gas and promote commercial production in shale gas reservoirs. Generally, Shale gas reservoir (SGR) is tight or ultratight formations,

with pore sizes ranging from 1–200 nm [6] and matrix intrinsic permeability from 10^{-9} – 10^{-3} mD [7,8]. The stress dependence of shale properties, for example, porosity and permeability, complicates the study even further [9]. Thus, researching gas transport mechanisms in organic shale nanopores is a very complex and challenging task for petroleum engineers [10,11].

Gas adsorption is a special storage form in SGRs, which can account for up to 85% of the original gas in place due to the very large surface area of a shale formation [4]. On one hand, adsorbed gas increases the recoverable shale gas reserves, because it will desorb from pore surfaces when pressure decreases [12–15]; on the other, adsorbed gas occupies a certain amount of flow paths and changes the effective hydraulic radius, which cannot be ignored for nanometer-scale transport studies [10,11]. Surface diffusion of adsorbed gas occurs under a chemical potential energy gradient in shale nanopores [16] and facilitates shale gas production. Considering the high reservoir pressure and surface heterogeneity, a surface diffusion model of adsorbed gas in nanopores of SGRs was established and analyzed by Wu et al. [17]. A new formulation of apparent permeability (AP) for gas transport in SGRs was proposed by Zhang et al. [18], which took surface diffusion into account. Wang et al. [19] established an AP model for gas transport in shale nanopores considering multiple effects, such as non-Darcy flow and surface diffusion.

Viscous flow and Knudsen diffusion of free gas are two important bulk phase gas transport mechanisms. Due to the breakdown of the continuum hypothesis in nanopores, the viscous seepage theory must be modified to satisfy slip boundaries. Klinkenberg [20] devised an empirical formulation to account for the slippage effect, which linked slippage permeability to intrinsic permeability, average pressure, and an empirical parameter b_k . After that, much effort has been made to obtain this parameter b_k theoretically or empirically [21–26]. Basing their work on the dynamic slippage concept, Ertekin et al. [23] established a new AP model considering the slippage effect. Skjetne and Auriault [27] made a further study on the gas slippage flow phenomenon in porous media (PM) on the basis of the Navier–Stokes equation.

Another type of slip model is based on slip boundary conditions (BCs), including the first and second-order modifications. The Maxwell slip model [28] is a first-order approximation from kinetic theory, based on which many other permeability models [25,26,29] have been established for tight and shale gas reservoirs. Second-order slip velocity models have been successively proposed to improve calculation precision. Hisa et al. [30] investigated molecular rarefaction effects through experiments and proposed a new slip BC that added a second-order term to the Maxwell model [28]. Basing their work on high-order slip BCs and asymptotic analysis, Beskok and Karniadakis [31] proposed another widely used second-order slip velocity model. Considering the location difference between slip surface and solid wall, Zhang et al. [32] improved the Beskok–Karniadakis (BK) slip model by introducing a new parameter γ to describe the distance between the slip surface and the solid wall. Niu et al. [33] made a new second-order gas-permeability correlation for shale gas slip flow based on the study of Zhang et al. [32]. In summary, slip velocity models can uniformly be expressed as:

$$u_{\text{slip}} = C_1 \lambda \left(\frac{\partial u}{\partial n} \right)_s + C_2 \lambda^2 \left(\frac{\partial^2 u}{\partial n^2} \right)_s \quad (1)$$

where u_{slip} is the velocity at the slip surface; λ is average mean free path of gas molecules; and C_1 and C_2 are two slip coefficients, the values of which are summarized in Table 1.

The values of some parameters in those slip velocity models, for example, the tangential momentum accommodation coefficient σ_v , can be very difficult to determine [39–41]. Although that coefficient is defined as the percentage of molecules reflected diffusively from solid walls, its physical meaning is still not very straightforward. The value has to be obtained by experiments or molecular dynamics (MD), which are also not easy tasks [41]. Besides, the slip velocity derived from those models may not be bounded, depending on specific situations [39,40], which may cause severe problems in numerical applications [42]. Except for Zhang et al. [32] and Niu et al. [33], all the studies in Table 1 ignored the distance between the slip surface and the solid wall. Meanwhile, in those studies,

gas molecules through a slip surface are assumed to be comprised of molecules from solid wall and the surface λ away from the solid wall, which account for the same percentage of 50% (that is, $n_\lambda = n_w = 0.5 n_s$). This assumption is also invalid when gas molecules are not uniformly distributed across the pipe section. The uneven molecule distribution, which can be attributed to the existence of gas molecular accumulation or adsorption near solid walls, has been proved by MD [32,33].

Table 1. Slip coefficients in different slip boundary conditions.

Reference	C_1	C_2
Maxwell [28]	$(2 - \sigma_v)/\sigma_v$	0
Hsia et al. [30]	$(2 - \sigma_v)/\sigma_v$	-1/2
Hwang et al. [34]	0.01807	$-0.676775(4/\pi)^{0.58734} Kn^{-0.82532}$
Beskok et al. [31]	$1/(1 - b Kn)$	0
Aubert et al. [35]	$(2 - \sigma_v)/\sigma_v$	-9/8
Bahukudumbi et al. [36]	$[1.2977 + 0.71851 \tan^{-1}(-1.17488 Kn^{0.58642})] (2 - \sigma_v)/\sigma_v$	0
Hadjiconstantinou [37]	1.1466	-0.647
Ng et al. [38]	1.15	$-0.25 Kn^{-0.65}$
Zhang HW et al. [32]	$[1 - (1 - \gamma)\sigma_v]/\sigma_v$	$(1 - \gamma)[1 - (1 - \gamma)\sigma_v]/(2\sigma_v)$

Note: σ_v is tangential momentum accommodation coefficient; Kn is Knudsen number; b is slip coefficient in B-K model [31]; γ is a parameter in Zhang's model to describe slip surface location.

In those slip velocity models, the content of molecules diffusively reflected from solid walls is artificially assumed to be σ_v , whereas $(1 - \sigma_v)$ is the ratio of molecules specularly reflected to incident molecules. However, in reality gas molecules do not rebound elastically from solid walls after colliding [39–41,43–45], due to the existence of attractive forces between gas and solid molecules. Gas molecules can be adsorbed on solid surfaces and then desorbed when the pressure decreases, causing an inelastic rebound. Therefore, a Langmuir slip BC more accurately describes the real slip phenomenon from the perspective of a physical meaning. Knudsen diffusion and surface diffusion are important gas transport mechanisms in shale nanopores. Although the Langmuir slip permeability (LSP) model for SGRs was first studied by Singh et al. [41], the results are not very convenient to apply. Besides, Knudsen/surface diffusion, real gas effects, geomechanical effects, and thermodynamics phase changes were also not considered in their research. Song et al. [46] pointed out that slippage flow, Knudsen diffusion, and surface diffusion were three gas transfer mechanisms in nanometer pores. However, the effects of slippage flow and Knudsen diffusion were broadly coupled together by the BK model [31] in their research, which ignored gas accumulation near pore walls and failed to distinguish the relative intensity of slippage flow and Knudsen diffusion in different conditions. Besides, the surface diffusion model in their study did not consider the effects of PM properties.

In this paper, considering gas-solid interaction, the slip phenomenon is described by the Langmuir slip BC [39–41], and a new slip model for bulk phase gas transport was established. Based our work on the LSP model, we also propose a new gas transport model coupling viscous flow, slippage effect, Knudsen diffusion, surface diffusion, and adsorption/desorption. Also taken into consideration were the real gas effect, stress dependence of physical properties, thermodynamics phase changes due to pore confinement, and dynamic adsorption layer thickness. The advantages of our LSP model over previous Maxwell-based ones are also illustrated. To make our gas transport model more applicable to practical situations, we re-expressed it in an AP form and upscaled it from a single capillary model to a porous media form, which coupled porosity and tortuosity into AP model and considered the effects of adsorbed gas volume on effective porosity.

2. Flow Mechanisms and Their Description in Nanopores

The three main gas storage forms in SGRs are free gas, adsorbed gas, and dissolved gas. Due to the nanometer-scale effect, bulk phase free gas can be transferred by slippage viscous flow under pressure gradient and by Knudsen diffusion under a concentration field. Meanwhile, adsorbed gas

can move from one site to another to achieve mass transport on pore surface by surface diffusion [47]. The typical gas storage and transport form in shale nanopores is shown in Figure 1.

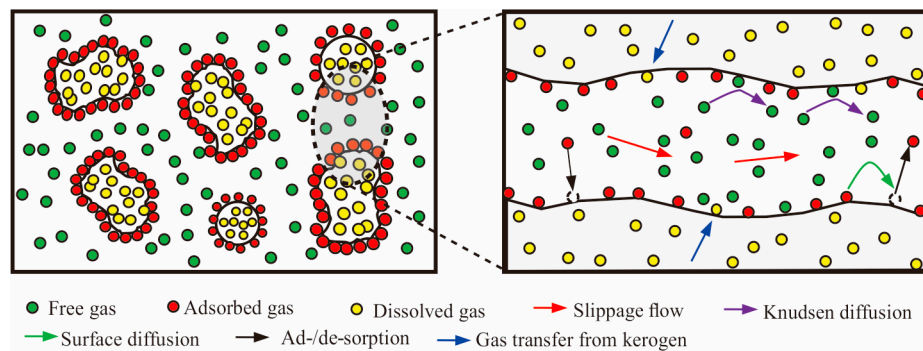


Figure 1. Storage form and flow mechanism of shale gas in nanopores.

2.1. Stress-Dependent Darcy Permeability

As is known, the intrinsic permeability of a nanometer capillary with a circular section can be given [19,46,48] as:

$$k_{\text{ins}} = \frac{r^2}{8} \quad (2)$$

where r is the radius of the capillary tube.

To take stress dependence into account, we adopt Gangi's model [46,49,50] to describe the permeability change under effective stress:

$$k_{\text{ins}\sigma} = k_0 \frac{[1 - (\frac{\sigma}{p_1})^m]^3}{[1 - (\frac{\sigma_0}{p_1})^m]^3}, \quad (3)$$

where k_0 is the formation permeability at original state, m^2 ; p_1 and m are parameters related to the pore stiffness and roughness respectively; σ_0 is effective stress of initial state, Pa; σ is the effective stress during production, which can be obtained by:

$$\sigma = p_s - \alpha p \quad (4)$$

where p_s is overburden formation pressure, Pa; α is Biot constant, dimensionless; p is reservoir pressure, Pa.

Considering the geomechanical impacts of formation compaction during reservoir depletion, we have the intrinsic permeability expression as follows by coupling Equations (2)–(4):

$$k_{\text{ins}\sigma} = \frac{r_0^2}{8} \frac{[1 - (\frac{p_c - \alpha p}{p_1})^m]^3}{[1 - (\frac{p_c - \alpha p_0}{p_1})^m]^3}. \quad (5)$$

2.2. LSP Modeling

The adsorption and desorption behaviors of shale gas have been studied in petroleum industry for a long time. However, the interfacial interaction between gas molecules and solid surfaces has failed to attract wide attention in the industry. Based our work on the Langmuir slip BC [39–41], we will establish a new LSP model considering gas molecule residence on solid surfaces when the gas-solid collision happens.

The Langmuir adsorption isotherm can be expressed in the following form [44]:

$$\theta = \frac{bp}{1 + bp} \quad (6)$$

where θ is the gas coverage ratio on a solid surface, dimensionless, and b is the Langmuir equilibrium adsorption constant, Pa^{-1} , which is usually expressed as the ratio of equilibrium adsorption rate to equilibrium desorption rate.

To unify our model with previous ones, the following expression of parameter b can be adopted [44]:

$$b = \frac{1}{4\omega Kn} \frac{1}{p_r} \quad (7)$$

where ω is a parameter related to gas-solid interaction; p_r is the reference pressure, Pa; and Kn is the Knudsen number, dimensionless, which can be written as the ratio of gas mean free path to characteristic length [11,51] as:

$$Kn = \frac{\lambda}{R_h} \quad (8)$$

The slip velocity BC could be expressed in the following form [39–41,52] once the surface coverage ratio is calculated:

$$u_s = \theta u_w + (1 - \theta)u_\lambda \quad (9)$$

where u_s is the slip surface velocity, m^2/s ; u_w is the velocity of solid wall, m^2/s ; and u_λ is gas velocity at the surface a mean free path away from the wall, m^2/s .

In SGRs, the velocity of the wall can be presumed as zero. Moreover, the reference velocity can also be chosen as the midstream value, the reason for which can be found in the study of Eu [53].

Therefore, the Langmuir slip BC can be obtained by coupling Equations (6) and (9):

$$u_s = \frac{1}{1 + bp} u(x, r = 0) \quad (10)$$

The Navier–Stokes equation can be adopted to describe the viscous incompressible Newtonian fluid flow [32,33] as:

$$\rho \left(\frac{\partial \vec{u}}{\partial t} + \vec{u} \cdot \nabla \vec{u} \right) = -\nabla p + \mu \nabla^2 \vec{u} + \rho \vec{g} \quad (11)$$

where ρ is the fluid density, kg/m^3 ; \vec{u} is the velocity field; μ is gas viscosity, $\text{Pa}\cdot\text{s}$; and $\rho \vec{g}$ is the gravity force.

Usually, for fluid flow in a nanometer circular capillary, the influence of $\rho \vec{g}$ is negligible. Besides, the value of $\partial \vec{u} / \partial t$ can be set to zero when the flow is under steady state. Taking the cylindrical coordinate system (see Figure 2) and ignoring the term of inertia force and mass force, the following Stokes equation is adopted to describe steady state Hagen–Poiseuille fluid flow [32,33,54]:

$$\frac{1}{r} \frac{d}{dr} \left(r \frac{du}{dr} \right) = \frac{1}{\mu} \frac{dp}{dx} \quad (12)$$

According to practical situations, the fluid velocity in nanopores should be a finite value. Thus, the following definite solution condition could be given:

$$u|_{r=0} < +\infty \quad (13)$$

By solving the Hagen–Poiseuille flow Equation (12), with the definite solution condition of Equations (10) and (13), the fluid velocity distribution in a circular tube could be obtained:

$$u(r) = -\frac{R^2}{4\mu} \frac{dp}{dx} \left[1 + \frac{4\omega p_r}{p} Kn - \left(\frac{r}{R} \right)^2 \right] \quad (14)$$

Integrating the velocity distribution u over the radius r , the flow rate can be calculated

$$Q = \int_0^R 2\pi r \cdot u(r) dr \quad (15)$$

Based on the expression of flow rate Q , we can get the permeability modification coefficient F according to the research of Sakhaee-Pour and Bryant [54] as:

$$F = \frac{Q(Kn)}{Q(Kn \rightarrow 0)} = 1 + \frac{8\omega p_r}{p} Kn. \quad (16)$$

Up to now, the establishment of the LSP model has been completed, which considers slippage effect, molecular residence on solid wall after collisions, and geomechanical effects of stress dependence during depressurization:

$$k_{\text{slip}} = F(p, Kn) k_{\text{ins}\sigma} \quad (17)$$

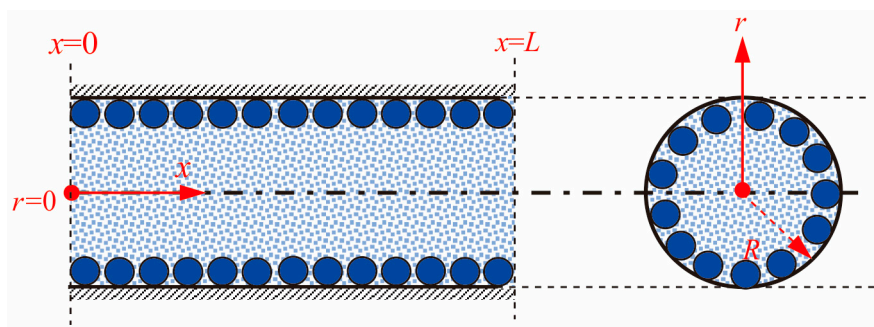


Figure 2. Schematic of fluid flow in circular capillary.

2.3. Knudsen Diffusion

Knudsen diffusion is another important transport mechanism in nanometer pores [55–58]. Considering solid surface roughness [18,59], we can express Knudsen diffusion in the following form:

$$J_k = -\delta^{D_f-2} M D_k \cdot \nabla c_g \quad (18)$$

where δ is the pore surface roughness, dimensionless; D_f is fractal dimension of pore surface, dimensionless; M is molar mass, kg/mol; J_k is Knudsen mass flux, kg/(m²·s); c_g is gas concentration, mol/m³; and D_k is the Knudsen diffusion coefficient, m²/s, the value of which is shown in Table 2.

According to the gas state equation, gas concentration C can be expressed with the consideration of real gas effect as:

$$c_g = \frac{p}{Z R_{\text{cst}} T} \quad (19)$$

where R_{cst} is the gas constant, 8.314 J/(mol·K).

Finally, the Knudsen diffusion flux can be expressed in terms of pressure gradient as:

$$J_k = -\delta^{D_f-2} \frac{M D_k}{RT} \cdot \frac{p c_g}{Z} \nabla p. \quad (20)$$

Table 2. Value of Knudsen diffusion coefficient in different models.

Number	D_k Expression	Reference
1	$D_k = 2r[8RT/(\pi M)]^{0.5}/3$	Igwe [56]
2	$D_k = 31.54(k_{\text{ins}})^{0.67}/M^{0.5}$	Ertekin et al. [23]
3	$D_k = 9700r(T/M)^{0.5}$	Ruthven [60]
4	$D_k = 4\sigma[\pi k_{\text{ins}}\varphi RT/(2M)]^{0.5}$	Florence et al. [24]

Note: T is temperature, K; φ is porosity.

2.4. Surface Diffusion

As we have introduced in Section 2.3, gas molecules could adsorb on solid surfaces and move under a chemical potential gradient [61]. Surface diffusion mass flux can be expressed [10,11,17,59] as:

$$J_s = -\frac{D_s C_s M}{p} \nabla p \quad (21)$$

where D_s is the surface diffusion coefficient, m^2/s , and C_s is the concentration of adsorbed gas, mol/m^3 .

Based on the research of Hwang and Kammermeyer [34] and combing the methane/carbon adsorption experiment data, the surface diffusion coefficient for methane could be given [11,16,52] as:

$$D_s = 8.29 \times 10^{-7} T^{0.5} \exp\left(-\frac{\Delta H^{0.8}}{RT}\right) \quad (22)$$

where ΔH is the equivalent adsorption heat, J/mol.

According to the Langmuir adsorption theory, the adsorbed gas concentration can be expressed as:

$$C_s = \frac{\rho_{\text{gsc}} G_L \theta_{\text{real}}}{M} \quad (23)$$

where G_L is the Langmuir volume, m^3/m^3 , and ρ_{gsc} is gas density at the standard condition, kg/m^3 .

Note that the expression of gas concentration C_s in Equation (23) includes the influence of the gas coverage ratio. Thus, there is no need to modify diffusion coefficient D_s when pressure changes, which differs from previous studies [10,11,17,59] and is very convenient in application.

In Equation (23), θ_{real} is the gas coverage ratio on solid surfaces considering the real gas effect and thermodynamics phase changes, which can be expressed as:

$$\theta_{\text{real}} = \frac{bp/Z}{1 + bp/Z} \quad (24)$$

2.5. Pore Confinement and the Real Gas Effect

A gas deviation factor Z is adopted to account for the real gas effect and thermodynamic phase changes of nanopore fluids due to the pore confinement effect. To calculate this parameter, critical pressure and temperature changes in nanometer-scale pores should be calculated first, which can be obtained by a modified van der Waals equation proposed by Islam et al. [46] in the following form [62]:

$$T_c = \frac{8}{27bR_{\text{cst}}} \left[a - 2\zeta^3 \varepsilon N^2 \frac{\zeta}{r_\sigma} \left(2.6275 - 0.6743 \frac{\zeta}{r_\sigma} \right) \right] \quad (25)$$

$$p_c = \frac{8}{27b^2} \left[a - 2\zeta^3 \varepsilon N^2 \frac{\zeta}{r_\sigma} \left(2.6275 - 0.6743 \frac{\zeta}{r_\sigma} \right) \right] \quad (26)$$

where T_c is pseudocritical temperature, K; p_c is pseudocritical pressure, MPa; a is the van der Waals energy parameter, 10^{-6} Pa·m⁶/mol²; b is the van der Waals volume parameter, 10^{-3} m³/mol; ζ is the Lennard–Jones size parameter, m; ε is the Lennard–Jones energy parameter, dimensionless; and N is Avogadro’s constant, 6.02×10^{23} .

Then, according to the corresponding state principle, pseudoreduced pressure and temperature are expressed as:

$$p_{pr} = \frac{p}{p_c} \quad (27)$$

and:

$$T_{pr} = \frac{T}{T_c} \quad (28)$$

where p_{pr} is the pseudoreduced pressure, dimensionless, the and T_{pr} is pseudoreduced temperature, dimensionless.

The gas deviation Z -factor can be solved out by the following correlation formula for high-pressure gases:

$$Z = (0.702 \times e^{-2.5T_{pr}})p_{pr}^2 - 5.524 \times e^{-2.5T_{pr}}p_{pr} + 0.044 \times T_{pr}^2 - 0.164 \times T_{pr} + 1.15 \quad (29)$$

Gas viscosity can be obtained by the following formula proposed by Izadmehr et al. [63]:

$$\mu = a \times T_{pr} + b \times p_{pr} + c \times \sqrt{p_{pr}} + d \times T_{pr}^2 + e \times \frac{p_{pr}}{T_{pr}} + f \quad (30)$$

The values of coefficients a through f are shown in Table 3.

Table 3. Values of correlation coefficients for viscosity calculation.

Coefficient	Value
a	0.00850507486545010
b	−0.00104065426590739
c	−0.00217777225933512
d	−0.000510724061609292
e	0.00595154429253907
f	−0.000548942531453252

2.6. Effect of Adsorbed Layer on Pore Radii

The effect of gas molecule adsorption on nanometer-scale pore radii is not negligible, because the molecules are large enough to change the effective hydraulic radius. During reservoir production, adsorption has two effects on permeability: (1) the hindering effects due to its occupation of flow paths and (2) enhancement due to pore enlargement after desorption during depressurization. Coupling Equations (2) and (3), we have the expression of pore radius under the effective stress σ :

$$r_{ins\sigma} = r_0 \left[\frac{1 - \left(\frac{\sigma}{p_1}\right)^m}{1 - \left(\frac{\sigma_0}{p_1}\right)^m} \right]^{1.5} \quad (31)$$

Assuming a monolayer adsorption on solid surfaces, the effect of adsorbed gas on pore radii can be given [46,59] by:

$$r_{eff} = r_{ins\sigma} - d_m \theta_{real} \quad (32)$$

where r_{eff} is the effective hydraulic radius considering the effect of stress dependence and gas adsorption on solid surface, m.

In the end, the permeability considering pore stress dependence and adsorbed gas occupation on flow paths as well as slippage effect can be written as:

$$k_{\text{eff}} = \frac{r_{\text{eff}}^2}{8} \quad (33)$$

where k_{eff} represents the effective permeability considering stress dependence and adsorption layer thickness, m^2 .

2.7. AP Modeling

To unify our model with continuum media flow equation of Darcy's law, Knudsen and surface diffusion flux were also transformed into the form of equivalent permeability. Comparing corresponding diffusion flux expression with Darcy's law, different types of equivalent permeability expressions could be obtained.

For slippage viscous flow, considering the effects of stress dependence and dynamic adsorption/desorption, the equivalent permeability could be expressed from the LSP model as:

$$k_{\text{slip}} = F(Kn, p) \cdot \frac{r_{\text{eff}}^2}{8} \quad (34)$$

In contrast to previous slip models, the slip coefficient F is not only a function of Knudsen number Kn , but also dependent on pore pressure.

For Knudsen diffusion, the equivalent permeability has the following form, where the Knudsen diffusion coefficient is determined by the method of Igwe [56]:

$$k_{\text{knudsen}} = \delta^{D_f-2} D_k c_g \mu \quad (35)$$

Similarly, the equivalent permeability of surface diffusion could be expressed as:

$$k_{\text{surface}} = D_s G_L \theta_{\text{real}} \frac{\mu Z}{p^2} \frac{T p_{\text{sc}}}{T_{\text{sc}}} \quad (36)$$

According to previous research by Xiong et al. [64], Wasaki and Akkutlu [51], and Javadpour [55], the AP can be written as the sum of bulk transport and adsorbed gas transport. Therefore, the AP of a single nanoscale capillary can be written as:

$$k_{\text{app}} = F(Kn, p) \cdot \frac{r_{\text{eff}}^2}{8} + \delta^{D_f-2} D_k c_g \mu + D_s G_L \theta_{\text{real}} \frac{\mu Z}{p^2} \frac{T p_{\text{sc}}}{T_{\text{sc}}} \quad (37)$$

2.8. Model Correlation Considering PM Properties

The AP expression of Equation (37) represents a single capillary (Figure 3b), without considering PM properties and their geomechanical effects during depressurization. Thus, it needs to be upscaled to incorporate the effective porosity and tortuosity [65] (Figure 3a) to represent numerous nanopores in SGRs.

Considering the existence of adsorbed gas on solid surfaces, the effective radius and area for bulk phase gas transport are r_{eff} and A_{eff} respectively; the radius and cross-section area of the single capillary are r_1 and A_1 respectively. Meanwhile, the length of a single capillary is l_1 and the permeability is k_1 . Correspondingly, the PM is assumed to be composed of n capillaries, with permeability k_t , cross section area A_t , and length l_t .

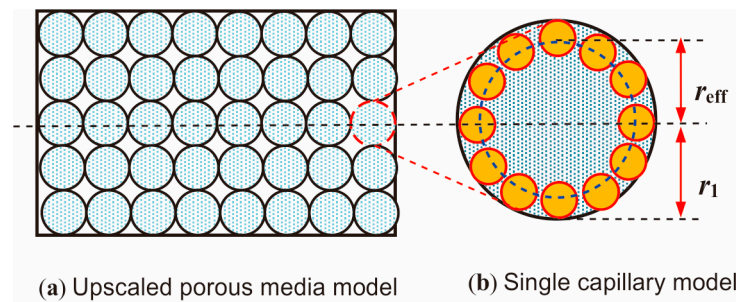


Figure 3. Scheme of upscaled porous media (UPM) model and single capillary model.

For bulk phase gas transport in n single capillaries without considering adsorbed gas, the volume flux can be given according to Darcy's law using the equivalent permeability conception as:

$$q_n = -nA_1 \frac{k_1}{\mu} \frac{dp}{dl_1}. \quad (38)$$

The volume flux of UPM (upscaled porous media) model is:

$$q_t = -A_t \frac{k_t}{\mu} \frac{dp}{dl_t}. \quad (39)$$

According to equivalent state, the volume flux calculated from Equations (38) and (39) should be the same, so we have:

$$k_t = \frac{nA_1}{A_t} \frac{dl_t}{dl_1} k_1 \quad (40)$$

From a physical meaning perspective, we have the following two expressions [66]

$$nA_1 = A_t \varphi \quad (41)$$

$$\tau = \frac{l_1}{l_t} \quad (42)$$

Coupling Equations (40)–(42), the relation between k_1 and k_t is obtained as:

$$k_t = \frac{\varphi}{\tau} k_1 \quad (43)$$

Considering the effect of adsorbed gas on porosity, we have:

$$\varphi_{\text{eff}} = \varphi \left(\frac{r_{\text{eff}}}{r_1} \right)^2 \quad (44)$$

Thus, the correction factor from single capillary model to UPM model for bulk phase gas is:

$$\gamma_b = \frac{\varphi}{\tau} \left(1 - \frac{r_{\text{ad}}}{r_1} \right)^2 \quad (45)$$

In Equation (45), r_{ad} is the thickness of the adsorption layer, which can account for the occupation of adsorbed gas in flow paths and the pore enlargement due to gas desorption during pressure-depletion production:

$$r_{\text{ad}} = d_m \theta_{\text{real}} \quad (46)$$

where d_m is the gas molecular diameter, m.

Assuming the cross section area for surface diffusion is A_s and taking similarly procedures as bulk gas transport for surface diffusion, the volume flux in n single capillaries is calculated as:

$$q_{ns} = -nA_s \frac{k_s dp}{\mu dl_1} \quad (47)$$

For surface diffusion in UPM model, the volume flux is:

$$q_{st} = -A_t \frac{k_{ts} dp}{\mu dl_t} \quad (48)$$

According to the single capillary model (Figure 3b), the ratio of A_s to A_1 is:

$$\frac{A_s}{A_1} = 1 - \left(\frac{r_{\text{eff}}}{r_1}\right)^2 \quad (49)$$

Coupling Equations (41) and (42) and Equations (47)–(49), we have the correction factor from single capillary to UPM model for surface diffusion as:

$$\gamma_s = \frac{\phi}{\tau} \left(1 - \left(1 - \frac{r_{\text{ad}}}{r_1}\right)^2\right) \quad (50)$$

In Equations (45) and (50), the tortuosity τ can be estimated by the empirical formula [18,67,68]

$$\tau = 1 + 0.63 \ln(1/\phi) \quad (51)$$

Finally, the AP considering PM properties and adsorbed gas occupation can be expressed as:

$$k_{\text{app}} = \gamma_b F(Kn, p) \cdot \frac{r_{\text{eff}}^2}{8} + \gamma_b \delta^{D_t-2} D_k c_g \mu + \gamma_s D_{\text{sur}} G_L \theta_{\text{real}} \frac{\mu Z T p_{\text{sc}}}{p^2 T_{\text{sc}}} \quad (52)$$

3. Model Validation

Currently, the use of Langmuir velocity slip BC for gas transport studies in SGRs is relatively rare and new in the petroleum industry. Thus, the accuracy of our LSP model, bulk phase gas transport model, single capillary model, and UPM model are all validated in this section.

First, the experimental data and lattice Boltzmann method (LBM) simulation results from Fathi et al. [69] are adopted in this section to validate our LSP model. The experimental data was collected from a routine gas uptake measurements using 5.68 mm size fragments. As can be seen from Figure 4, the matching results from three different sources are reasonable, which can prove the accuracy of our LSP model. Corresponding fitting parameters are presented in Table 4. Then, model comparison was done among first-order correlation [28], second-order correlation [30], corrected second-order correlation [33], and our LSP model (defining $\omega = 0.6$, $p_D = 1$, $\sigma_v = 0.6$, and $C = 0.55$), as can be seen in Figure 5. During the slip flow regime, the first and second-order correlation results are much higher than corrected second-order correlations and our LSP results, whereas corrected second-order correlation results overlap with the LSP results. This is because the first and second-order correlations assumed elastic gas–solid collisions and uniform distribution of gas molecules across the cross-section area of nanopores.

The corrected second-order correlation method considered the gas accumulation effects near solid surfaces according to MD, whereas our LSP model considered gas adsorption on solid surfaces for slip flow study. Gas accumulation and adsorption both narrow flow paths and hinder gas transport in small pores. The first- and second-order correlation methods ignored the hindering effect and may overestimate the slip permeability in formation evaluation.

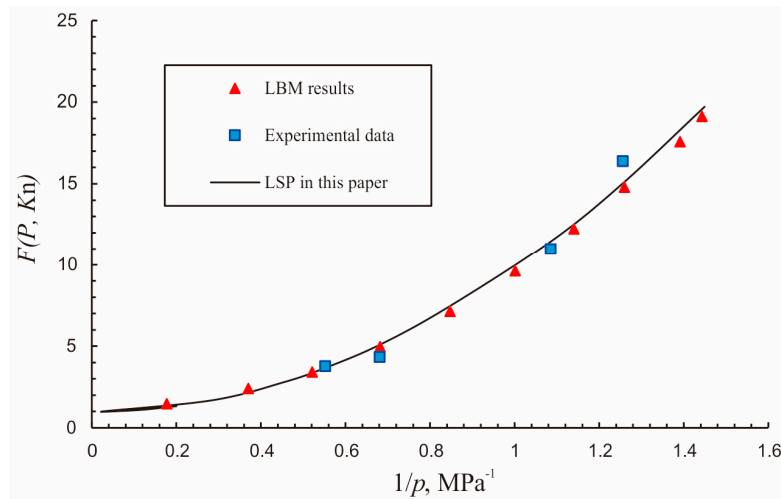


Figure 4. Validation of our LSP model by experimental data and numerical simulation.

Table 4. Input parameters for LSP model validation.

Parameter	Value	Parameter	Value
Overburden pressure, p_c	90 MPa	Pore radius, r	10 nm
Pore pressure, p	0.69 to 40 MPa	Pressure at original state, p_0	80 MPa
Pore roughness parameter, m	0.5	Gas constant, R_{cst}	8.314 J/(mol·K)
Temperature, T	353 K	Biot constant, α	1
Pore stiffness parameter, p_1	150 MPa	Reference pressure for LSP, p_r	1 MPa
Adsorption parameter, ω	0.1		

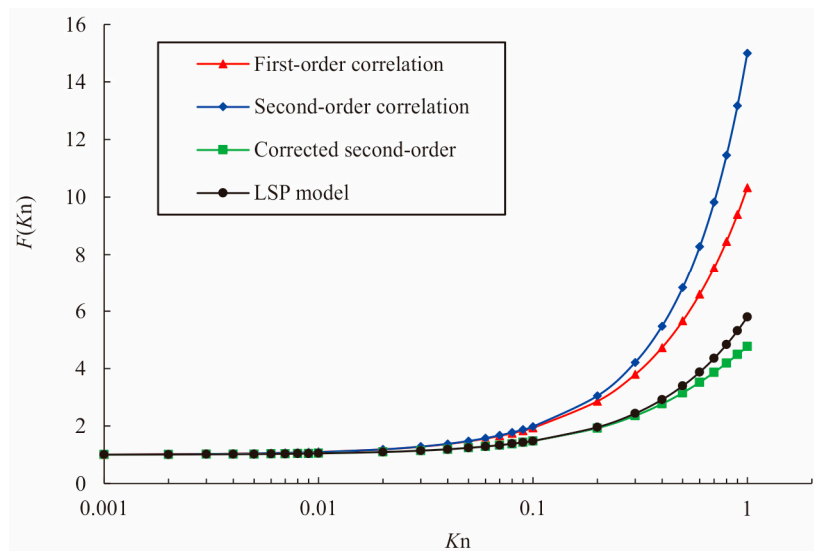


Figure 5. Model comparison from different slip boundary conditions.

Then, to validate the bulk phase gas transport model, we compared the results from our model to those published data from linearized Boltzmann solutions [70] and experimental data [71]. Note that bulk phase gas is defined as that transported by slip viscous flow and Knudsen diffusion, and bulk phase permeability is defined as the sum of slip permeability k_{slip} and the equivalent Knudsen permeability $k_{knudsen}$. As can be seen from Figure 6, three different data sources adequately match with each other.

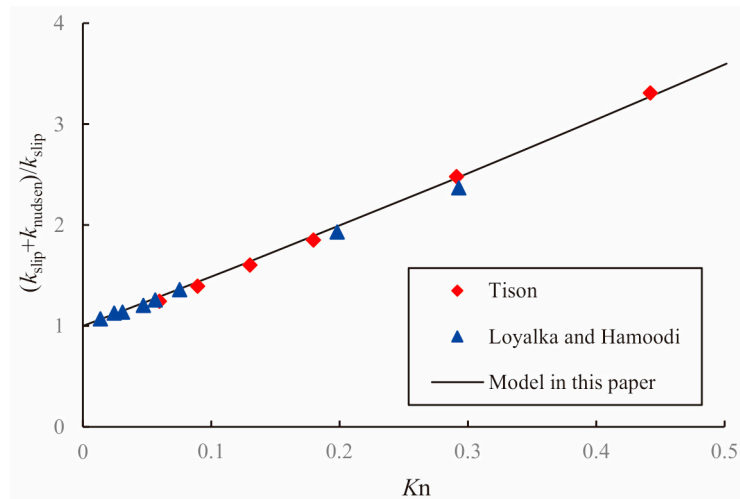


Figure 6. Bulk phase gas-permeability model validation compared with published data [70,71].

Further, the AP (considering bulk phase and adsorbed gas transporting) and bulk phase permeability (without considering surface diffusion) from our model (defining pore pressure $p = 2$ MPa, formation temperature $T = 383$ K, $\omega = 0.2$, reference pressure $p_r = 0.1$ MPa, pore stiffness parameter $m = 0.5$, pore fractal dimension $D_f = 2.6$, and pore roughness $\delta = 0.25$) is compared with those from the generalized lattice Boltzmann model in Wang et al. [72]. Clearly, both AP and bulk phase gas permeability match the Lattice Boltzmann method (LBM) results very well in different pore size conditions, as shown in Figure 7. Surface diffusion plays an important role in small pores and throats, but it can be ignored when pore radius is larger than 20 nm in this condition.

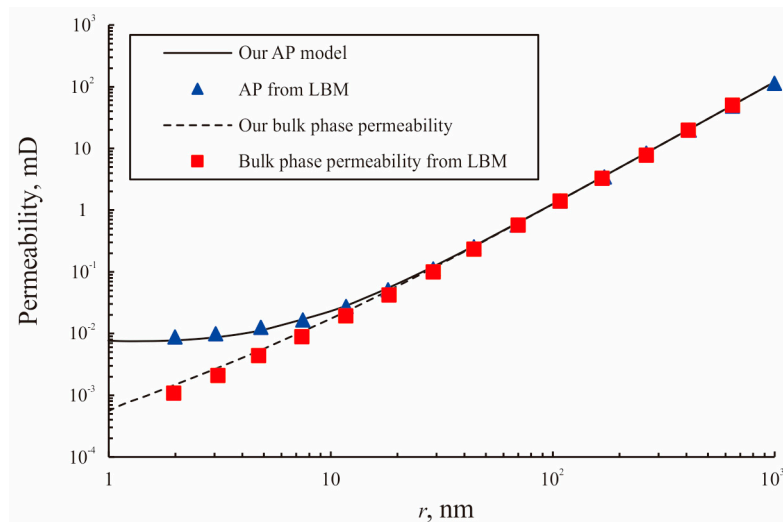


Figure 7. Model validation by comparing our model with LBM results.

Finally, model comparison was done for AP models to further validate the proposed model's correctness. The calculated results from different models are shown in Figure 8 (corresponding parameters used for comparison are presented in Table 5). The model of Michel et al. [73] describes only bulk phase gas transport and ignores adsorbed gas. Thus, the results are quite lower than those of other models and basically constant with pressure changes. Because both adsorbed gas and bulk phase gas are considered, the results from Xiong et al. [64], Wasaki et al. [9], and our UPM model display a similar changing trend; that is, an increase of k_{app}/k_{ins} as pressure decreases. However, our model results are similar to Xiong et al. [64] at low pressures and tend to match those of Wasaki et al. [9]

as pressure increases. This is because inelastic gas–solid collisions, thermodynamic phase changes due to pore confinement, the dynamic hindering effect of adsorbed gas, real gas effects, and geomechanical effects are simultaneously considered in our model. Besides, Knudsen diffusion and the slippage effect were discussed separately in our model, whereas in the other two models they are treated by a modification function of Knudsen number Kn . Furthermore, surface diffusion is influenced in real time by pressure and temperature in our model, whereas constant diffusion coefficients were chosen for whole production time in the other two models. All these factors led to the different decreasing trend of AP models in Figure 8.

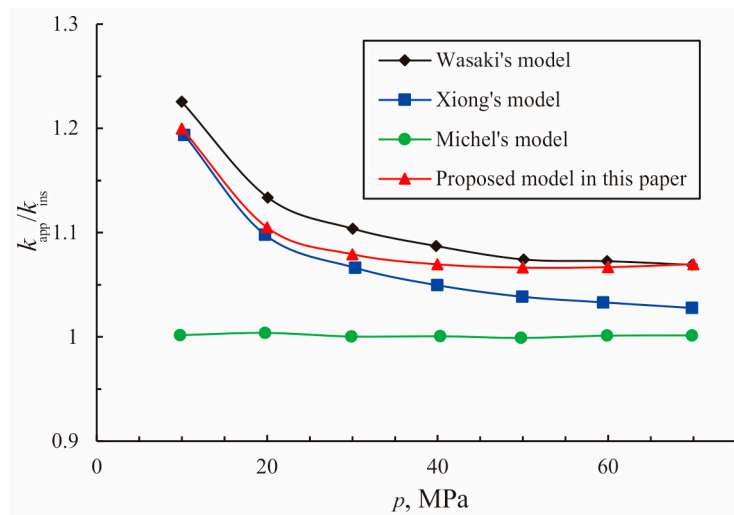


Figure 8. Comparison of our model with previous studies.

Table 5. Parameters used for model comparison.

Parameter	Value	Parameter	Value
Gas type	CH ₄	Pore radius, r	30 nm
Pore pressure, p	10–70 MPa	Porosity, ϕ	0.060
Overburden pressure, p_c	90 MPa	Reference pressure, p_r	1 MPa
Adsorption parameter, ω	2	Temperature, T	414 K
Pore roughness parameter, m	0.5	Pore roughness, δ	0.7
Fractal dimension of pore surface, D_f	2.5		

4. Results and Discussion

In this section, the parameters sensitivity analysis will be done in different conditions, including the influences of pore radius, pressure, temperature, effective stress, and other parameters on the flux of each fluid flow mechanism; that is, viscous flow, Knudsen diffusion, and surface diffusion. Corresponding parameters used in our model are listed in Table 6.

With an increase in pore radius, slip flow permeability (Figure 9) as well as its contribution to total flux (Figure 10) also increases. In large pores ($r > 20$ nm) with pressures larger than 5 MPa, the effect of stress dependence is more obvious than that of the slippage effect. Thus, during the depressurization production, the slip permeability becomes less and less as effective stress increases. In small pores, the slippage effect dominates compared to stress dependence, and the slippage permeability increases as the pore pressure decreases. When the pore pressure is small enough, the permeability enhancement of the slippage effect is stronger than the permeability abatement of stress dependence in all pores, as shown in Figure 9.

Table 6. Input parameters of gas and formation for model analysis.

Parameter	Value	Parameters	Value
Gas type	CH ₄	Pore radius, r	0.5–100 nm
Pore pressure, p	1–70 MPa	Porosity, ϕ	0.05
Langmuir pressure, p_L	13.79 MPa	Gas molar weight, M	0.016 kg/mol
Temperature, T	373 K	Biot constant, α	1
Fractal dimension, D_f	2.7	Reference pressure, p_r	1 MPa
Surface roughness, δ	0.4	Gas constant, R_{cst}	8.314 J/(mol·K)
Equivalent adsorption heat, ΔH	16,000 J/mol	vdW energy parameter, a	0.22998 m ⁶ Pa/mol ²
Pore stiffness parameter, p_1	150 MPa	vdW energy parameter, b	4.28 × 10 ⁻⁵ m ³ /mol
Pore roughness parameter, m	4	Lennard–Jones size parameter, ζ	3.73 × 10 ⁻⁹ m
Adsorption parameter, ω	2	Lennard–Jones size parameter, ϵ	2.0434 × 10 ⁻²¹
Avogadro's constant, N	6.02 × 10 ²³	Langmuir volume, G_L	20 m ³ /m ³

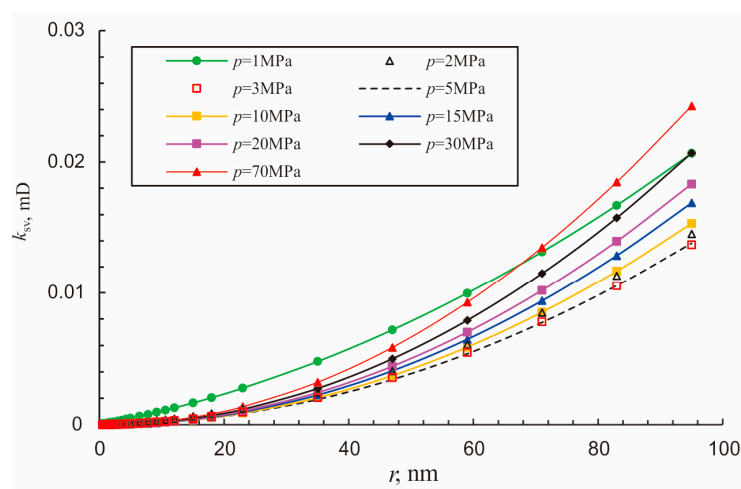
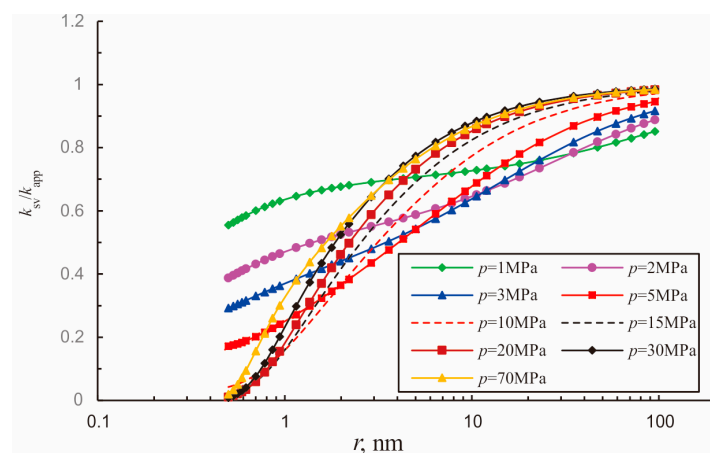
**Figure 9.** Equivalent permeability of slip viscous flow in different conditions.**Figure 10.** Contribution of slip viscous flow to total flux in different conditions.

Figure 10 shows that the contribution of slip flow increases with an increase in pore radius, and the increasing trend is faster in high-pressure and small pore radius conditions. In small pores, low pressure condition has a larger contribution than high pressure, while high pressure has a bigger contribution than small pressure in large pores. The slip flow contribution increases as pressure increases in pores with radii larger than 30 nm, although it displays complex changing rules in pores with radii smaller than 10 nm.

Knudsen diffusion becomes stronger with an increase in pore radius and a decrease in pressure (Figure 11). This is because the equivalent permeability of Knudsen diffusion is influenced mainly by the Knudsen diffusion coefficient in a certain pressure and temperature condition. For a constant pore radius, Knudsen diffusion increases with the decrease in pore pressure. Although gas viscosity increased as pressure increases, Knudsen diffusion permeability k_{Knudsen} is more influenced by compressibility coefficient c_g , the two of which have a nearly inverse proportion relation. The contribution of Knudsen diffusion to total flux is very complex in small pores, as shown in Figure 12. Generally, that contribution decreases with pore radius in low-pressure conditions ($p < 5$ MPa), whereas it increases rapidly at first and slowly decreases later in high-pressure conditions ($p > 10$ MPa).

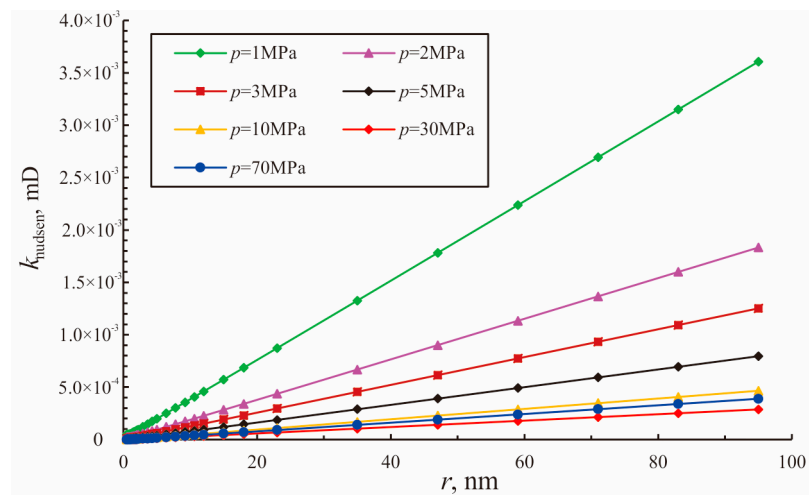


Figure 11. Equivalent permeability Knudsen diffusion in different conditions.

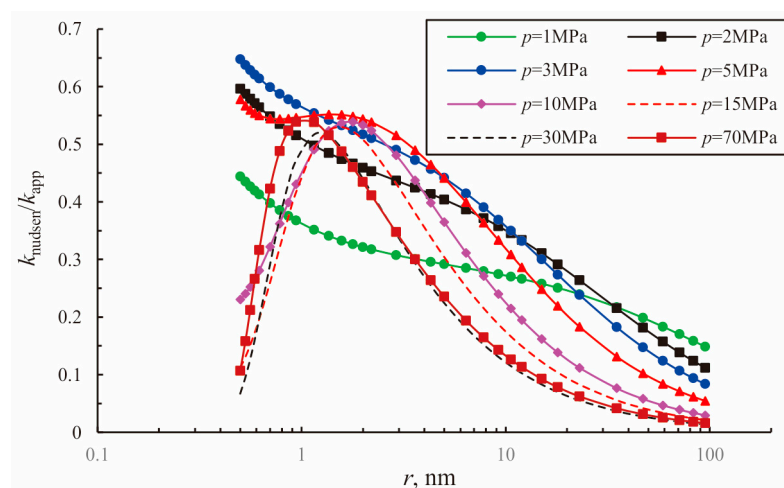


Figure 12. The contribution of Knudsen diffusion to total flux in different conditions.

The change of surface diffusion with pore radius in high-pressure ($p > 10$ MPa) conditions is quite different from that in low-pressure ($p < 5$ MPa) conditions (Figure 13). It increases at first and decreases later as pore radius increases in low-pressure conditions, whereas it has a persistent decrease under high pressure. Actually, the detailed changing trend of surface diffusion intensity is not important, because its contribution is quite limited in large pore radii ($r > 3$ nm), no matter whether the value is low or high (Figure 14). However, its contribution to total flux is prominent in small pores. This is because it is advantageous for the occurrence of surface diffusion in small pores, when the porosity of PM is a constant. Meanwhile, the contribution of surface diffusion can be ignored in low-pressure

conditions, although pore radii are small enough for the occurrence of surface diffusion. This is because adsorbed gas concentration is a function of the gas coverage ratio, which is very small in low-pressure conditions (Figure 15) and weakens the occurrence of surface diffusion.

Generally, non-Darcy flow mechanisms are dominant mainly in low-pressure and small pore radius conditions (Figure 16). With an increase in pore radii, the influence of the non-Darcy flow weakens and the flow tends to be viscous flow only.

For gas flow in pores with radii greater than 0.7 nm, the non-Darcy flow becomes more and more obvious during depressurization production. However, in contrast with previous studies, for gas flow in pores with radii less than 0.7 nm, with pressure decreasing, the non-Darcy flow effect is stronger at first, and then weakens abruptly. This is because surface diffusion dominates the flow in small pores when the pressure is larger than 10 MPa, but plays only a slight role when the pressure is less than 10 MPa (Figure 14).

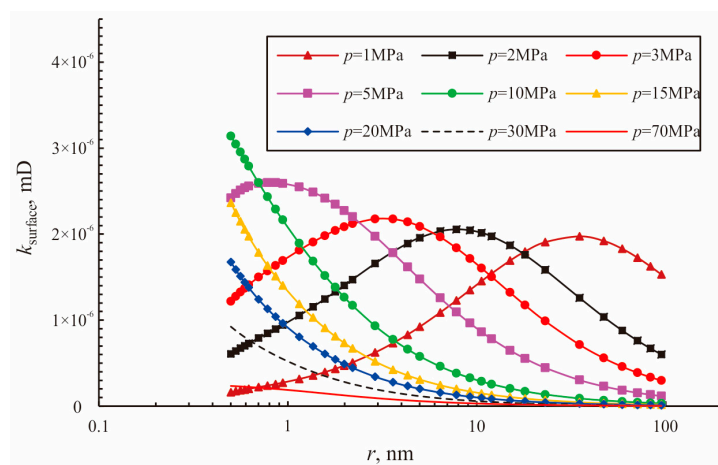


Figure 13. Equivalent permeability of surface diffusion in different conditions.

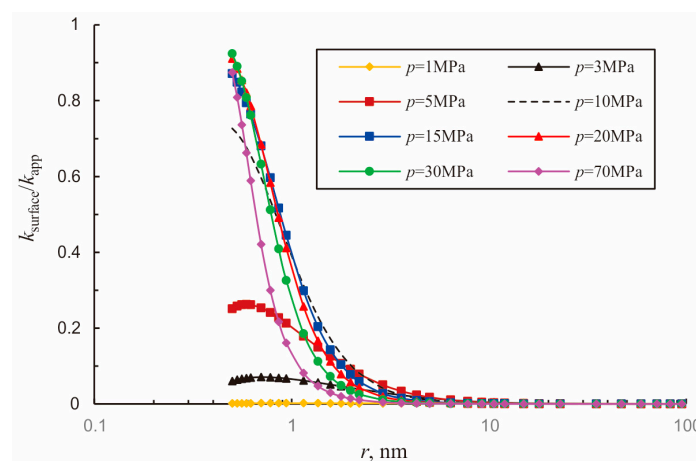


Figure 14. Contribution of surface diffusion to total flux in different conditions.

As shown in Figure 17, the AP increases as pressure decreases in small pores, because the effect of the non-Darcy flow is stronger in low-pressure and small radius conditions. In large pores and throats, the AP is obviously influenced by both the non-Darcy flow effect and the geomechanical effect of stress dependence. The permeability decreases as pressure decreases at first due to stress sensitivity, and increases abruptly at low pressures, because the influence of the non-Darcy flow is more obvious than the geomechanical effects.

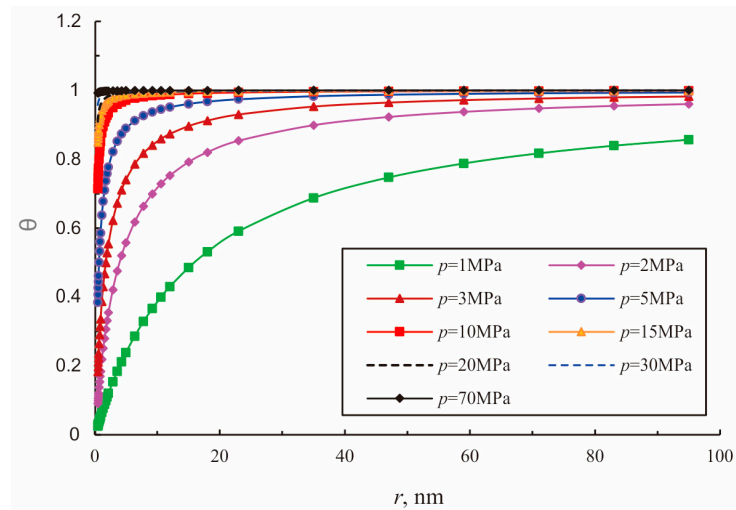


Figure 15. Gas coverage ratio under different pore size and pressure conditions.

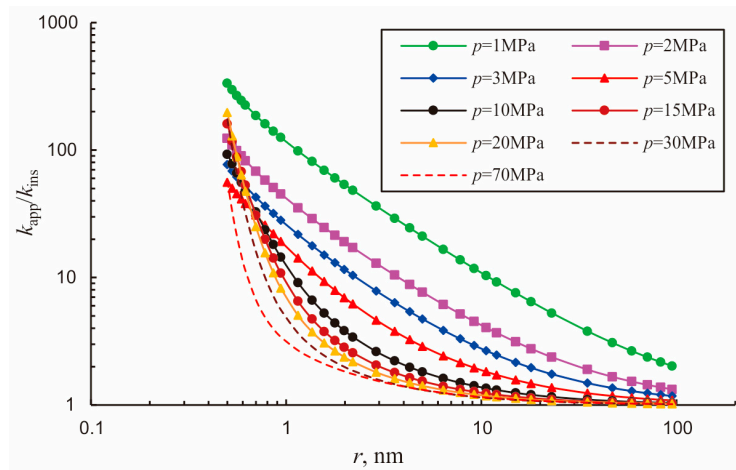


Figure 16. Ratio of AP to intrinsic permeability in different conditions.

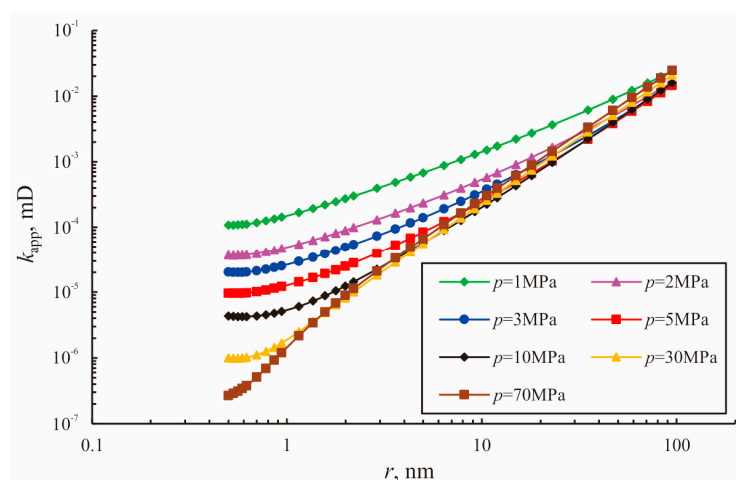


Figure 17. AP in different pore and pressure conditions.

5. Conclusions

In this paper, a coupled AP model is established by introducing a Langmuir slip BC, simultaneously considering viscous flow, slippage effect, Knudsen diffusion, surface diffusion and adsorption/desorption. Both single capillary and capillary bundle models are established, which were validated by experimental data and LBM results. Coupled into the AP model were the effects of real gas, stress dependence, thermodynamic phase changes due to pore confinement, adsorbed layer thickness, pore enlargement due to gas desorption, surface roughness, and inelastic gas-solid collisions. Based on the AP model, the following conclusions can be made:

1. The LSP model considers both gas slippage and gas adsorption effects on solid surfaces in nanopores. Gas slippage has a permeability enhancement effect, whereas gas adsorption effect is important in the estimation of permeability because adsorbed gas narrows flow paths.
2. The non-Darcy flow is prominent in small pore size and low-pressure conditions and displays an abnormal increase with a decrease of pore radii in small pores due to the coexistence of surface diffusion and Knudsen diffusion.
3. The geomechanical effect has a greater influence on AP of larger pores than the non-Darcy effect, whereas the AP of small pores is more influenced by the non-Darcy flow effect.
4. The intensity of slip flow, Knudsen diffusion, and surface diffusion as well as their contribution to total flux was studied quantitatively; these intensities change with great complexity due to the combined effects of real gas, thermodynamics phase changes, and geomechanics.

Acknowledgments: This work was supported by the National Natural Science Foundation of China (Key Program) (Grant No. 51534006), the National Science Fund for Distinguished Young Scholars of China (Grant No. 51125019), the National Natural Science Foundation of China (Grant No. 5170427) and the Scientific Research Starting Project of SWPU (No. 2015QHZ003). The authors also appreciate the reviewers and editors whose critical comments were very helpful in preparing this article.

Author Contributions: The original idea of this paper was proposed by Liehui Zhang and Baochao Shan. The mathematical model and solution were derived by Baochao Shan and Yulong Zhao. The results analysis was conducted by Jia Du and Jun Chen. The curves were plotted by Xiaoping Tao. The whole paper was written by Baochao Shan and Yulong Zhao, while the design of the structure and English improvement were finished by Liehui Zhang.

Conflicts of Interest: The authors declare no conflicts of interest.

Nomenclature

u_{slip}	velocity at the slip surface, m/s;
λ	average mean free path of gas molecules, m;
C_1, C_2	slip coefficients;
r	radius of the capillary tube, m;
k_0	formation permeability at original state, m^2 ;
$p_{1,m}$	parameters related to the pore stiffness and roughness respectively;
σ_0	effective stress of initial state, Pa;
σ	effective stress during production;
p_s	overburden formation pressure, Pa;
α	Biot constant, dimensionless;
p	reservoir pressure, Pa;
θ	gas coverage ratio on a solid surface, dimensionless;
b	Langmuir equilibrium adsorption constant, Pa^{-1} ;
ω	parameter related to gas-solid interaction;
p_r	reference pressure, Pa;

Kn	Knudsen number, dimensionless;
u_s	slip surface velocity, m^2/s ;
u_w	velocity of solid wall, m^2/s ;
u_λ	gas velocity at the surface a mean free path away from the wall, m^2/s ;
ρ	fluid density, kg/m^3 ;
\vec{u}	velocity field;
μ	gas viscosity, $Pa \cdot s$;
$\vec{\rho g}$	gravity force;
δ	pore surface roughness, dimensionless;
D_f	fractal dimension of pore surface, dimensionless;
M	molar mass, kg/mol ;
J_k	Knudsen mass flux, $kg/(m^2 \cdot s)$;
c_g	gas concentration, mol/m^3 ;
D_k	Knudsen diffusion coefficient, m^2/s ;
R_{cst}	gas constant, $8.314 J/(mol \cdot K)$;
D_s	surface diffusion coefficient, m^2/s ;
C_s	concentration of adsorbed gas, mol/m^3 ;
ΔH	equivalent adsorption heat, J/mol ;
G_L	Langmuir volume, m^3/m^3 ;
ρ_{gsc}	gas density at the standard condition, kg/m^3 ;
T_c	pseudocritical temperature, K ;
p_c	pseudocritical pressure, MPa ;
a	VdW energy parameter, $10^{-6} Pa \cdot m^6/mol^2$;
b	VdW volume parameter, $10^{-3} m^3/mol$;
ζ	Lennard–Jones size parameter, m ;
ϵ	Lennard–Jones energy parameter, dimensionless;
N	Avogadro’s constant, 6.02×10^{23}
p_{pr}	pseudoreduced pressure, dimensionless,
T_{pr}	pseudoreduced temperature, dimensionless;
r_{eff}	effective hydraulic radius, m ;
k_{eff}	effective permeability, m^2 ;
d_m	gas molecular diameter, m

References

1. Zhang, D.L.; Zhang, L.H.; Guo, J.J.; Zhou, Y.H.; Zhao, Y.L. Research on the production performance of multistage fractured horizontal well in shale gas reservoir. *J. Nat. Gas Sci. Eng.* **2015**, *26*, 279–289. [[CrossRef](#)]
2. Zhao, Y.L.; Shan, B.C.; Zhang, L.H.; Liu, Q.G. Seepage Flow Behaviors of Multi-stage Fractured Horizontal Well in Arbitrary Shaped Shale Gas Reservoirs. *J. Geophys. Eng.* **2016**, *13*, 674–689. [[CrossRef](#)]
3. Zhang, R.H.; Zhang, L.H.; Wang, R.H.; Zhao, Y.L.; Huang, R. Simulation of a Multistage Fractured Horizontal Well with Finite Conductivity in Composite Shale Gas Reservoir through Finite-Element Method. *Energy Fuels* **2016**, *30*, 9036–9049. [[CrossRef](#)]
4. Zhang, L.H.; Guo, J.J.; Tang, H.M. *Fundamental of Shale Gas Reservoir Development*; Petroleum Industry Press: Beijing, China, 2014. (In Chinese)
5. Zhang, L.H.; Shan, B.C.; Zhao, Y.L.; Tang, H.M. Comprehensive Seepage Simulation of Fluid Flow in Multi-scaled Shale Gas Reservoirs. *Transp. Porous Media* **2017**, *1*–26. [[CrossRef](#)]
6. Zhou, Z.; Wang, X.Z.; Yin, G.; Yuan, S.S.; Zeng, S.J. Characteristics and genesis of the (Sinian) Dengying Formation reservoir in Central Sichuan, China. *J. Nat. Gas Sci. Eng.* **2016**, *29*, 311–321. [[CrossRef](#)]
7. Loucks, R.G.; Reed, R.M.; Ruppel, S.C.; Jarvie, D.M. Morphology, genesis and distribution of nanometer-scale pores in siliceous mudstone of the Mississippian Barnett shale. *J. Sediment. Res.* **2009**, *79*, 848–861. [[CrossRef](#)]
8. Wang, F.P.; Reed, R.M. Pore networks and fluid flow in gas shales. In Proceedings of the SPE Annual Technology Conference and Exhibition, New Orleans, LA, USA, 4–7 October 2009; Society of Petroleum Engineers: Richardson, TX, USA, 2009.
9. Wasaki, A.; Akkutlu, I.Y. Permeability of organic-rich shale. *SPE J.* **2015**, *20*. [[CrossRef](#)]

10. Wu, K.L.; Chen, Z.X.; Li, X.F.; Xu, J.Z.; Li, J.; Wang, K.; Wang, H.; Wang, S.H.; Dong, X.H. Flow behavior of gas confined in nanoporous shale at high pressure: Real gas effect. *Fuel* **2017**, *205*, 173–183.
11. Wu, K.L.; Chen, Z.X.; Li, X.F. Real gas transport through nanopores of varying cross-section type and shape in shale gas reservoirs. *Chem. Eng. J.* **2015**, *281*, 813–825. [[CrossRef](#)]
12. Fathi, E.; Akkutlu, Y.I. Matrix heterogeneity effects on gas transport and adsorption in coalbed and shale gas reservoirs. *Transp. Porous Media* **2009**, *80*, 281–304.
13. Brown, M.; Ozkan, E.; Raghavan, R.; Kazemi, H. Practical solutions for pressure-transient responses of fractured horizontal wells in unconventional shale reservoirs. *SPE Reserv. Eval. Eng.* **2011**, *14*, 663–673. [[CrossRef](#)]
14. Zhao, Y.L.; Zhang, L.H.; Zhao, J.Z.; Luo, J.X.; Zhang, B.N. “Triple porosity” modeling of transient well test and rate decline analysis for multi-fractured horizontal well in shale gas reservoirs. *J. Pet. Sci. Eng.* **2013**, *110*, 253–262. [[CrossRef](#)]
15. Ozkan, E.; Brown, M.; Raghavan, R.; Kazemi, H. Comparison of fractured-horizontal-well performance in tight sand and shale reservoirs. *SPE Reserv. Eval. Eng.* **2011**, *14*, 248–259. [[CrossRef](#)]
16. Guo, L.; Peng, X.F.; Wu, Z.S. Dynamical characteristics of methane adsorption on monolith nanometer activated carbon. *J. Chem. Ind. Eng.* **2008**, *59*, 2726–2732. (In Chinese)
17. Wu, K.; Li, X.; Wang, C.; Yu, W.; Chen, Z. A Model for Surface Diffusion of Adsorbed Gas in Nanopores of Shale Gas Reservoirs. In Proceedings of the Offshore Technology Conference, Houston, TX, USA, 4–7 May 2015. [[CrossRef](#)]
18. Zhang, L.J.; Li, D.L.; Lu, D.T.; Zhang, T. A new formulation of apparent permeability for gas transport in shale. *J. Nat. Gas Sci. Eng.* **2015**, *23*, 221–226. [[CrossRef](#)]
19. Wang, J.; Liu, H.Q.; Wang, L.; Zhang, H.L.; Luo, H.S.; Gao, Y. Apparent permeability for gas transport in nanopores of organic shale reservoirs including multiple effects. *Int. J. Coal Geol.* **2015**, *152*, 50–62. [[CrossRef](#)]
20. Klinkenberg, L.J. The permeability of porous media to liquids and gases. In *API Drilling and Production Practice*; American Petroleum Institute: Washington, DC, USA, 1941.
21. Jones, F.O.; Owens, W.W. A laboratory study of low-permeability gas sands. *J. Pet. Technol.* **1980**, *32*, 1631–1640. [[CrossRef](#)]
22. Sampath, K.; Keighin, C.W. Factors affecting gas slippage in tight sandstones of cretaceous age in the Ninta Basin. *J. Pet. Technol.* **1982**, *34*, 2715–2720. [[CrossRef](#)]
23. Ertekin, T.; King, G.A.; Schwerer, F.C. Dynamic gas slippage: A unique dual-mechanism approach to the flow of gas in tight formations. *SPE Form. Eval.* **1986**, *1*, 43–52. [[CrossRef](#)]
24. Florence, F.A.; Rushing, J.; Newsham, K.E.; Blasingame, T.A. Improved permeability prediction relations for low permeability sands. In Proceedings of the Rocky Mountain Oil & Gas Technology Symposium, Denver, CO, USA, 16–18 April 2007; Society of Petroleum Engineers: Richardson, TX, USA, 2007.
25. Javadpour, F. Nanopores and apparent permeability of gas flow in mudrocks (shales and siltstone). *J. Gas Can. Pet. Technol.* **2009**, *48*, 16–21. [[CrossRef](#)]
26. Civan, F. Effective correlation of apparent gas permeability in tight porous media. *Transp. Porous Media* **2010**, *82*, 375–384. [[CrossRef](#)]
27. Skjetne, E.; Auriault, J.L. Homogenization of wall-slip gas flow through porous media. *Transp. Porous Media* **1999**, *36*, 293–306. [[CrossRef](#)]
28. Maxwell, J. On stresses in rarefied gases arising from inequalities of temperature. *Proc. R. Soc. Lond.* **1878**, *27*, 304–308. [[CrossRef](#)]
29. Darabi, H.; Eftehad, A.; Javadpour, F.; Sepehrnoori, K. Gas flow in ultra-tight shale strata. *J. Fluid Mech.* **2012**, *710*, 641–658. [[CrossRef](#)]
30. Hsia, Y.T.; Domoto, G.A. An experimental investigation of molecular rarefaction effects in gas lubricated bearing at ultra-low clearances. *J. Tribol.* **1983**, *105*, 120–129. [[CrossRef](#)]
31. Beskok, A.; Karniadakis, G.E. A model for flows in channels, pipes, and ducts at micro and nano scales. *Microscale Thermophys. Eng.* **1999**, *3*, 43–77.
32. Zhang, H.W.; Zhang, Z.; Zheng, Y.; He, H. Corrected second order slip boundary condition for fluid flows in nanochannels. *Phys. Rev. E* **2010**, *81*, 066303. [[CrossRef](#)] [[PubMed](#)]
33. Niu, C.; Hao, Y.; Li, D.; Lu, D. Second-Order Gas-Permeability Correlation of Shale during Slip Flow. *SPE J.* **2014**. [[CrossRef](#)]

34. Hwang, C.C.; Fung, R.F.; Yang, R.F.; Weng, C.I.; Li, W.L. A new modified Reynolds equation for ultrathin film gas lubrication. *IEEE Trans. Magn.* **1996**, *32*, 344–347.
35. Aubert, C.; Colin, S. High order boundary conditions for gaseous flows in rectangular microducts. *Microscale Thermophys. Eng.* **2001**, *5*, 41–54.
36. Bahukudumbi, P.; Beskok, A. A phenomenological lubrication model for the entire Knudsen regime. *J. Micromech. Microeng.* **2003**, *13*, 873. [[CrossRef](#)]
37. Hadjiconstantinou, N.G. Comment on Cercignani's second-order slip coefficient. *Phys. Fluids* **2003**, *15*, 2052–2354. [[CrossRef](#)]
38. Ng, E.Y.; Liu, N. A multicoefficient slip corrected Reynolds equation for micro-thin film gas Lubrication. *Int. J. Rotat. Mach.* **2005**, *2005*, 105–111. [[CrossRef](#)]
39. Myong, R.S. Gaseous slip models based on the Langmuir adsorption isotherm. *Phys. Fluids* **2004**, *16*, 104–117. [[CrossRef](#)]
40. Myong, R.S. A generalized hydrodynamic computational model for rarefied and microscale diatomic gas flows. *J. Comput. Phys.* **2004**, *195*, 655–676. [[CrossRef](#)]
41. Singh, H.; Javadpour, F. Langmuir slip-Langmuir sorption permeability model of shale. *Fuel* **2016**, *164*, 28–37. [[CrossRef](#)]
42. Beskok, A.; Karniadakis, G.E. Modeling separation in rarefied gas flows. *AIAA Pap.* **1997**, *97*, 1883.
43. Dushman, S. *Scientific Foundations of Vacuum Techniques*; Wiley: New York, NY, USA, 1962.
44. Langmuir, I. Surface chemistry. *Chem. Rev.* **1933**, *13*, 147–191. [[CrossRef](#)]
45. Adamson, A.W. *Physical Chemistry of Surfaces*; Wiley: New York, NY, USA, 1982.
46. Song, W.; Yao, J.; Li, Y.; Sun, H.; Zhang, L.; Yang, Y.; Zhao, J.; Sui, H. Apparent gas permeability in an organic-rich shale reservoir. *Fuel* **2016**, *181*, 973–984. [[CrossRef](#)]
47. Zhang, L.H.; Shan, B.C.; Zhao, Y.L.; Guo, J.J.; Tang, H.M. Establishment of apparent permeability model and seepage flow model for shale reservoir. *Lithol. Reserv.* **2017**, *29*, 108–118. (In Chinese)
48. Civan, F.; Devegowda, D.; Sigal, R.F. Critical evaluation and improvement of methods for determination of matrix permeability of shale. In Proceedings of the SPE Annual Technical Conference and Exhibition, New Orleans, LA, USA, 30 September–2 October 2013; Society of Petroleum Engineers: Richardson, TX, USA, 2013.
49. Gangi, A.F. Variation of whole and fractured porous rock permeability with confining pressure. *Int. J. Rock Mech. Min. Sci. Geomech. Abstr.* **1978**, *15*, 249–257. [[CrossRef](#)]
50. Kwon, O.; Kronenberg, A.K.; Gangi, A.F.; Johnson, B.; Herbert, B.E. Permeability of illite-bearing shale: 1. Anisotropy and effects of clay content and loading. *J. Geophys. Res. Solid Earth* **2004**, *109*. [[CrossRef](#)]
51. Zhao, J.Z.; Li, Z.Q.; Hu, Y.Q.; Ren, L.; Tao, Z.W. The impacts of microcosmic flow in nanoscale shale matrix pores on the gas production of a hydraulically fractured shale-gas well. *J. Nat. Gas Sci. Eng.* **2016**, *29*, 431–439. [[CrossRef](#)]
52. Sheng, M.; Li, G.S.; Huang, Z.W.; Tian, S.C. Shale gas transient flow with effects of surface diffusion. *Acta Petrol. Sin.* **2014**, *35*, 347–352. (In Chinese)
53. Eu, B.C.; Khayat, R.E.; Billing, G.D.; Nyeland, C. Nonlinear transport coefficients and plane Couette flow of a viscous, heat-conducting gas between two plates at different temperatures. *Can. J. Phys.* **1987**, *65*, 1090–1103. [[CrossRef](#)]
54. Sakhaee-Pour, A.; Bryant, S. Gas Permeability of Shale. *PE Reserv. Eval. Eng.* **2012**, *15*. [[CrossRef](#)]
55. Javadpour, F.; Fisher, D.; Unsworth, M. Nanoscale gas flow in shale gas sediments. *J. Gas Can. Pet. Technol.* **2007**, *46*, 55–61. [[CrossRef](#)]
56. Igwe, G.J.I. *Gas Transport Mechanism and Slippage Phenomenon in Porous Media*; Paper SPE 16479 Present at the SPE Conference; Society of Petroleum Engineers: Richardson, TX, USA, 1987.
57. Zhao, Y.L.; Zhang, L.H.; Xiong, Y.; Zhou, Y.H.; Liu, Q.G.; Chen, D. Pressure response and production performance for multi-fractured horizontal wells with complex seepage mechanism in box-shaped shale gas reservoir. *J. Nat. Gas Sci. Eng.* **2016**, *32*, 66–80. [[CrossRef](#)]
58. Lin, D.; Wang, J.; Yuan, B.; Shen, Y.H. Review on gas flow and recovery in unconventional porous rocks. *Adv. Geo-Energy Res.* **2017**, *1*, 39–53. [[CrossRef](#)]

59. Wu, K.L.; Chen, Z.X.; Li, X.F.; Guo, C.H.; Wei, M.Z. A model for multiple transport mechanisms through nanopores of shale gas reservoirs with real gas effect–adsorption-mechanic coupling. *Int. J. Heat Mass Transf.* **2016**, *93*, 408–426. [[CrossRef](#)]
60. Ruthven, D.M. *Principles of Adsorption & Adsorption Processes*; John Wiley and Sons: Hoboken, NJ, USA, 1984; pp. 80–109.
61. Fathi, E.; Akkutlu, I.Y. Nonlinear Sorption Kinetics and Surface Diffusion Effects on Gas Transport in Low-permeability Formations. In Proceedings of the SPE Annual Technical Conference and Exhibition, New Orleans, LA, USA, 4–7 October 2009. [[CrossRef](#)]
62. Islam, A.W.; Patzek, T.W.; Sun, A.Y. Thermodynamics phase changes of nanopore fluids. *J. Nat. Gas Sci. Eng.* **2015**, *25*, 134–139. [[CrossRef](#)]
63. Izadmehr, M.; Shams, R.; Ghazanfari, M.H. New correlations for predicting pure and impure natural gas viscosity. *J. Nat. Gas Sci. Eng.* **2016**, *30*, 364–378. [[CrossRef](#)]
64. Xiong, X.; Devegowda, D.; Villazon, M.; German, G.; Sigal, R.F.; Civan, F. A fully-coupled free and adsorptive phase transport model for shale gas reservoirs including non-Darcy flow effects. In Proceedings of the SPE Annual Technical Conference and Exhibition Society of Petroleum Engineers, San Antonio, TX, USA, 8–10 October 2012; Society of Petroleum Engineers: Richardson, TX, USA, 2012.
65. Cai, J.C.; Wei, W.; Hu, X.Y.; Wood, D.A. Electrical conductivity models in saturated porous media: A review. *Earth-Sci. Rev.* **2017**, *171*, 419–433. [[CrossRef](#)]
66. Cai, J.C.; Perfect, E.; Cheng, C.-L.; Hu, X.Y. Generalized modeling of spontaneous imbibition based on Hagen-Poiseuille flow in tortuous capillaries with variably shaped apertures. *Langmuir* **2014**, *30*, 5142–5151. [[CrossRef](#)] [[PubMed](#)]
67. Comiti, J.; Renaud, M. A new model for determining mean structure parameters of fixed beds from pressure drop measurements: application to beds packed with parallelepipedal particles. *Chem. Eng. Sci.* **1989**, *44*, 1539–1545. [[CrossRef](#)]
68. Cai, J.C.; Yu, B.M. A discussion of the effect of tortuosity on the capillary imbibition in porous media. *Transp. Porous Media* **2011**, *89*, 251–263. [[CrossRef](#)]
69. Fathi, E.; Tinni, A.; Akkutlu, I.Y. Shale Gas Correction to Klinkenberg Slip Theory. In Proceedings of the SPE Americas Unconventional Resources Conference, Pittsburgh, PA, USA, 5–7 June 2012. [[CrossRef](#)]
70. Loyalka, S.K.; Hamoodi, S.A. Poiseuille flow of a rarefied gas in a cylindrical tube: solution of linearized Boltzmann equation. *Phys. Fluids A Fluid Dyn.* **1990**, *2*, 2061–2065. [[CrossRef](#)]
71. Tison, S.A. Experimental data and theoretical modeling of gas flows through metal capillary leaks. *Vacuum* **1993**, *44*, 1171–1175. [[CrossRef](#)]
72. Wang, J.J.; Chen, L.; Kang, Q.J.; Rahman, S.S. Apparent permeability prediction of organic shale with generalized lattice Boltzmann model considering surface diffusion effect. *Fuel* **2016**, *181*, 478–490. [[CrossRef](#)]
73. Michel Villazon, G.G.; Sigal, R.F.; Civan, F.; Devegowda, D. Parametric Investigation of Shale Gas Production Considering Nano-Scale Pore Size Distribution, Formation Factor, and Non-Darcy Flow Mechanisms. In Proceedings of the SPE Annual Technical Conference and Exhibition, Denver, CO, USA, 30 October–2 November 2011. [[CrossRef](#)]

